CellPress

Chem Catalysis

Perspective

Parallels between enzyme catalysis, electrocatalysis, and photoelectrosynthesis

Daiki Nishiori,[1,2] Brian L. Wadsworth,[1,2] and Gary F. Moore[1,*]

SUMMARY

Catalysts are central to accelerating chemistry in biology and technology. In biochemistry, the relationship between the velocity of an enzymatic reaction and the concentration of chemical substrates is described via the Michaelis-Menten model. The modeling and benchmarking of synthetic molecular electrocatalysts are also well developed. However, such efforts have not been as rigorously extended to photoelectrosynthetic reactions, where, in addition to chemical substrates and charge carriers, light is a required reagent. In this perspective, we draw parallels between concepts involving enzyme catalytic efficiency, the benchmarking of molecular electrocatalysts, and the performance of photoelectrosynthetic assemblies, while highlighting key differences, assumptions, and limitations.

The bigger picture

Challenges and opportunities:

- Cutting the tie between fossil-resource consumption and the manufacturing of fuels and chemical feedstocks is critical to mitigating the impacts of anthropogenic climate change. Materials that use sunlight to power chemical transformations enable opportunities to develop a sustainable energy future and green chemical manufacturing processes.
- Biology offers inspiration for designing and understanding the performance of human-engineered catalysts and materials for energy transduction. However, not every aspect of nature should be a target of chemical mimicry as there are fundamental differences between the operating principles of biological assemblies and their inspired, technological counterparts.
- An improved understanding of catalysis, including similarities and differences, across enzymatic, electrocatalytic, and photoelectrosynthetic materials is central to addressing contemporary energy challenges for science and the imagination.

INTRODUCTION

The synthesis of chemical compounds using photoelectrochemical methods is an active area of research, offering strategies to produce fuels and other value-added products with limited environmental impact.[1,2] In this vein, both photoanodes and photocathodes have been developed for driving oxidation and reduction half-reactions, respectively. Approaches to building such constructs include directly integrating semiconductors that harvest solar energy with electrocatalysts that lower the energy input required for powering selected chemical transformations at a desired rate.[3–7] The electrocatalytic components can be molecular/homogeneous or heterogeneous,[8] but in both cases the resulting composite materials are inherently heterogeneous.

Herein, we provide a contextual overview of the Michaelis-Menten model[9–11] for describing reactions catalyzed by enzymes. This is followed by a summary of benchmarking techniques established for characterizing the performance of molecular electrocatalysts and molecular-electrocatalyst-modified conducting electrodes.[12–18] These established approaches are then compared and contrasted with those emerging to describe photoelectrosynthetic reactions occurring at electrocatalyst-modified semiconducting electrodes that use light as a reagent and driving force.[19–25] Unlike the determination of enzyme catalytic efficiency and the benchmarking of molecular electrocatalysts, there is currently no established framework for extracting values of the kinetic and thermodynamic parameters required to make consistent comparisons between catalysts operating in photoelectrosynthetic constructs. When the maximum turnover frequency (TOF_{max}) a catalyst can achieve is not limited by the flux of photons or chemical substrate, it should be possible to ascertain the relevant benchmarking parameters using existing electrochemical techniques.[12] However, in practice, such conditions have proved difficult to achieve.

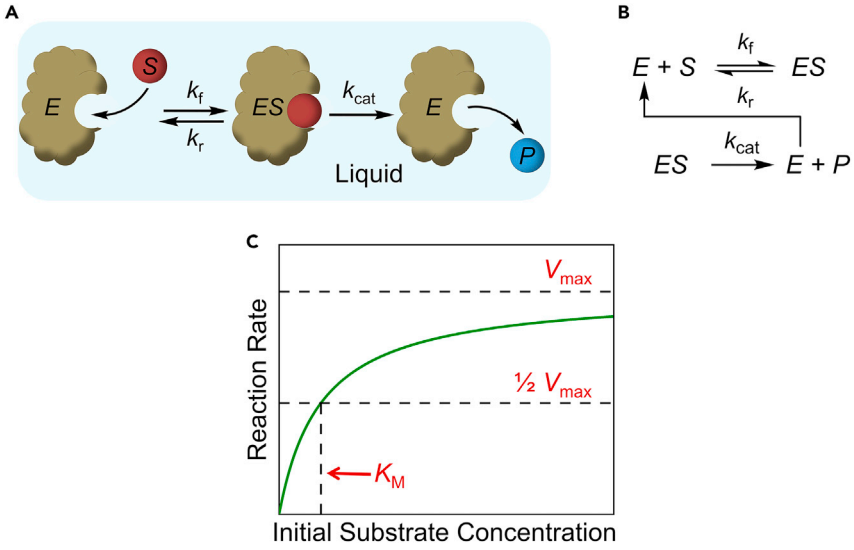

Figure 1. Overview of an enzymatic reaction

(A) A schematic depicting an enzymatic reaction where an enzyme (*E*) binds with a chemical substrate (*S*) to form an enzyme-substrate (*ES*) complex, which in turn releases the product (*P*) and regenerates the enzyme. The kinetics are governed by forward (k_f) and reverse (k_r) rate constants describing the binding and unbinding of *S*, respectively, as well as a rate constant for catalysis (k_{cat}).

(B) A reaction scheme for enzyme catalysis.

(C) A plot of the rate of an enzymatic reaction versus the initial concentration of chemical substrate ([*S*]). The maximum reaction velocity (V_{max}), half the maximum reaction velocity ($\frac{1}{2}$ V_{max}), and the Michaelis constant (K_M), representing [*S*] required to achieve $\frac{1}{2}$ V_{max}, are indicated with dashed lines.

ENZYMATIC CATALYSIS

The notion that enzymatic reactions are initiated by the formation of a chemical bond between an enzyme (a bio-molecular catalyst) and a chemical substrate is widely attributed to Victor Henri.[26] This idea provided a foundation for later efforts by Leonor Michaelis and Maud Menten describing the kinetics of invertase.[9,10] In the Michaelis-Menten model, an enzyme, *E*, binds a substrate, *S*, to form an enzyme-substrate, *ES*, complex, which then releases the product, *P*, and regenerates *E*.[27] Alternatively, the *ES* complex can release *S* and regenerate *E*. This overall process is represented schematically in Figure 1. In their original analysis, Michaelis and Menten applied a rapid pre-equilibrium approximation, meaning the substrate and enzyme are assumed to be in instantaneous chemical equilibrium with the *ES* complex. Thus, the rates of enzyme-substrate binding and unbinding are set equal over the course of the reaction, and the substrate unbinding is fast compared with the formation of product by the *ES* complex. Under these conditions, the concentration of the *ES* complex can be relatively high over the course of the reaction (see Figure 1B),[9,10] and the velocity (v), which is the rate of the enzymatic reaction, is expressed using Equations 1A and 1B:

$$v = \frac{d[P]}{dt} = \frac{V_{max}[S]}{K_d + [S]} \quad \text{(Equation 1A)}$$

$$K_d = \frac{k_r}{k_f} \quad \text{(Equation 1B)}$$

where V_{max} is the maximum reaction velocity (which is equal to the product of the catalytic rate constant, k_{cat}, and the initial concentration of enzyme, $[E]_0$) and K_d is the dissociation constant of the *ES* complex (which is equal to the ratio of reverse and forward rate constants k_r/k_f).

[1]School of Molecular Sciences and the Biodesign Institute Center for Applied Structural Discovery (CASD), Arizona State University, Tempe, AZ, USA

[2]These authors contributed equally

*Correspondence: gary.f.moore@asu.edu

https://doi.org/10.1016/j.checat.2021.09.008

An alternative steady-state analysis of enzymatic catalysis was later put forward by George E. Briggs and John B. S. Haldane.[11] In this approach, the rate of enzyme-substrate formation is set equal to the rate of enzyme-substrate consumption, meaning the concentration of *ES* remains relatively constant and low over the course of the reaction, as the activated complex is consumed almost as soon as it is formed. Under these conditions, the rate of product formation is described as shown in Equations 2A and 2B:

$$\upsilon = \frac{d[P]}{dt} = \frac{V_{max}[S]}{K_M + [S]} \quad \text{(Equation 2A)}$$

$$K_M = \frac{k_r + k_{cat}}{k_f} \quad \text{(Equation 2B)}$$

where K_M is the Michaelis constant, which defines the initial concentration of chemical substrate required for an enzyme to function at half its maximum velocity ($\frac{1}{2}$ V_{max}). As the initial concentration of chemical substrate is increased beyond the value of K_M, the reaction rate approaches the limiting velocity of V_{max} (Figure 1C). The ratio k_{cat}/K_M is used as a measurement of catalytic efficiency that provides an index for comparing the relative rates of an enzyme acting on alternative and/or competing substrates.[28] However, comparisons of k_{cat}/K_M values between different enzymes without carefully specifying limitations can result in invalid comparisons and misleading conclusions.[29]

HOMOGENEOUS MOLECULAR ELECTROCATALYSIS

In the area of homogeneous molecular electrocatalysis, benchmarking metrics have been established for characterizing the relatively large number and diversity of complexes being developed to address contemporary energy challenges.[12,13] During an electrocatalytic process, a catalyst, *C*, is activated via an electron-transfer reaction occurring at an electrode. Consistent with Marcus-Hush-Levich theory[30–32] and the Butler-Volmer equation,[33] the rate of this electron-transfer step is governed by a potential-dependent (i.e., a driving-force-dependent) heterogeneous electron-transfer rate constant, k_{et}, that is unique for each electrode/catalyst pair. The activated form of the catalyst, *C′*, can be formed via reductive activation of a catalyst for steering cathodic half-reactions as depicted in Figure 2, or via oxidative activation of a catalyst for steering anodic half-reactions. Following its formation, *C′* reacts with a chemical substrate, *S*, in a chemical step to form the product, *P*, with kinetics governed by a potential-independent rate constant, k_{cat}. For one-electron, one-substrate electrocatalytic reactions, k_{cat} can represent a rate constant associated with a single rate-limiting chemical step. For more complex, multi-electron, multi-chemical step reactions, k_{cat} can represent a global/observed rate constant associated with a rate-limiting chemical step or summation of steps involved in a catalytic cycle.[12,15,18,19]

The benchmarking of homogeneous molecular electrocatalysts requires determination of intrinsic catalytic properties that are independent of the characteristics of an electrochemical cell.[13] This is achieved via comparisons of catalytic Tafel plots (Figure 2D) relating the turnover frequency (TOF) of a molecular catalyst to an overpotential (η),[33] where η is defined as the difference in absolute value between the applied working electrode potential (E_{app}) and the equilibrium potential of the reaction being catalyzed (E_{eq}), as shown in Equation 3:[12]

$$\eta = \left| E_{app} - E_{eq} \right| \quad \text{(Equation 3)}$$

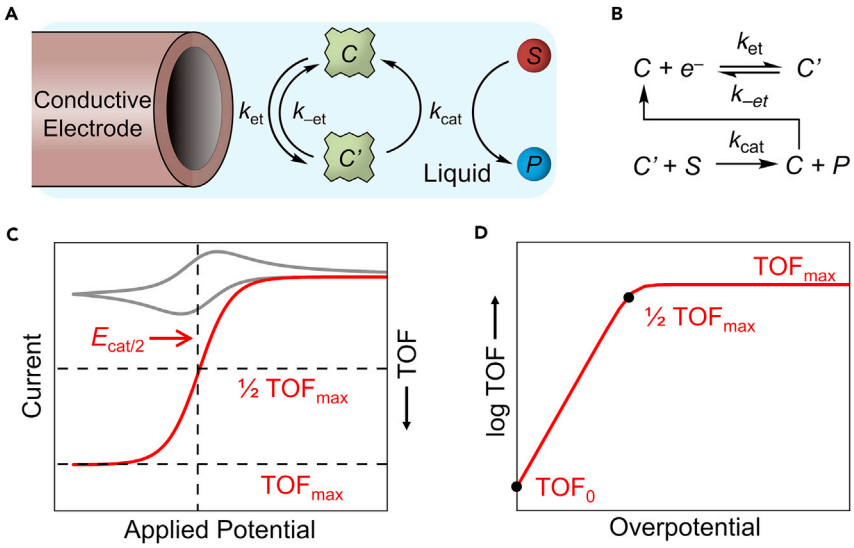

Figure 2. Overview of an electrocatalytic reaction involving a molecular (homogeneous) catalyst and a stationary electrode

(A) A schematic depicting homogeneous molecular electrocatalysis where transfer of electrons (e^-) between a conductive electrode and catalyst (*C*) produces the activated form of the catalyst (*C'*), which in turn reacts with a chemical substrate (*S*) to form the product (*P*) and regenerate *C*. The kinetics are governed by potential-dependent forward (k_{et}) and reverse (k_{-et}) electron-transfer rate constants, as well as a potential-independent catalytic rate constant (k_{cat}).

(B) A reaction scheme for electrocatalysis.

(C) Voltammograms associated with either the interconversion between oxidized and reduced forms of an electroactive species in solution (i.e., a duck-shaped voltammogram) (gray), or a catalytic reaction involving a fast and irreversible catalytic step where the overall concentration of chemical substrate is relatively high and thus remains essentially the same as the bulk concentration (i.e., an S-shaped voltammogram) (red). The maximum turnover frequency (TOF_{max}), half the maximum turnover frequency ($\frac{1}{2}$ TOF_{max}), and the potential required to achieve half the maximum turnover frequency ($E_{cat/2}$) are indicated with dashed lines.

(D) A catalytic Tafel plot constructed for a molecular electrocatalyst (see related text for further details).

As indicated in Equation 4, the TOF is the ratio of moles of product produced over a set unit of time in which the catalyst is stable ($N_{product}$), versus the moles of total catalysts ($C + C'$) contained within the reaction-diffusion layer (N_{cat}), not the bulk solution:[12]

$$TOF = \frac{N_{product}}{N_{cat}} \qquad \text{(Equation 4)}$$

For electrocatalytic transformations, where the value of k_{et} is a function of the applied bias, the electrode can be polarized at potentials where the rate of interfacial electron transfer is sufficiently greater than the rate of chemical catalysis. When the electrode activity is limited only by kinetics associated with chemical catalysis, and not limitations due to electron-transfer kinetics or mass-transfer phenomena, all of the catalysts at the electrode surface are effectively in their activated forms and the concentration of chemical substrate at the electrode surface is approximately equal to its bulk concentration. Under these conditions, the waveform of the resulting voltammogram is referred to as S-shaped, and the plateau current of the voltammogram (i_{cat}) will not increase upon increasing the scan rate because the effective concentration of activated catalysts is maximized (see Figure 2C).[18]

Thus, i_{cat} provides information on the per catalytic site TOF_{max}, which is equal to k_{cat} as shown in Equations 5A and 5B:

$$i_{cat} = nFA[C]\sqrt{D_{cat}n'TOF_{max}} \quad \text{(Equation 5A)}$$

$$TOF_{max} = k_{cat} = k'_{cat}[S]^x \quad \text{(Equation 5B)}$$

where n is the number of electron-transfer steps occurring at the electrode per electrocatalytic cycle, n' is the equivalents of catalyst required for turnover,[15] F is the Faraday constant, A is the electrode surface area, and D_{cat} is the diffusion coefficient of the catalyst. In these equations, k_{cat} is a pseudo-first-order rate constant that is the product of k'_{cat} and $[S]^x$, where k'_{cat} is a rate constant for catalysis taking into account the order of the reaction (x) with respect to the concentration of chemical substrate.

Unlike V_{max}, which is zero order with respect to the concentration of chemical substrate, TOF_{max} can be non-zero order with respect to the concentration of chemical substrate (see Equation 5B), meaning its value can increase upon increasing the concentration of chemical substrate. Nonetheless, substrate-independent TOF_{max} values (i.e., upper limits of TOF_{max}) have been determined.[34,35] In these measurements, i_{cat} reaches a limiting value that is independent of further increasing the concentration of chemical substrate as well as the scan rate. This implies the catalysts in the reaction-diffusion layer are operating at their maximum TOF_{max}. Further increasing the concentration of substrate will not enhance the reaction rate if the reaction has become zero order with respect to chemical substrate.

For reactions that are first order in catalyst, the relationship between TOF and η for most catalytic reaction mechanisms[18] is given by Equation 5C:

$$TOF = \frac{TOF_{max}}{1+\exp\left[\frac{F}{RT}\left(E_{app}-E_{cat/2}\right)\right]} = \frac{TOF_{max}}{1+\exp\left[\frac{F}{RT}\left(E_{eq}-E_{cat/2}\right)\right]\exp\left(-\frac{F}{RT}\eta\right)} \quad \text{(Equation 5C)}$$

where R is the gas constant, T is the absolute temperature, and $E_{cat/2}$ is the half-wave potential of the S-shaped wave (i.e., the potential at which half the maximum current ($i_{cat/2}$) is achieved). The asymptotic value of the TOF is the TOF_{max}, and its value is independent of the applied potential as well as the concentration of catalyst.[12] Unlike TOF, which is parametrized by an applied potential, TOF_{max} is a limiting value constrained by a potential-independent rate constant. By extension, the kinetic parameter TOF_{max} provides further physical meaning to the thermodynamic benchmarking parameter $E_{cat/2}$; it is the potential required to activate half the total number of catalysts in the reaction-diffusion layer.

Juxtaposed to TOF_{max}, TOF_0 is an extrapolated TOF at $\eta = 0$ (i.e., where the applied potential equals the equilibrium potential of the reaction being catalyzed). Their relationship is defined by Equation 5D:

$$TOF_0 = TOF_{max}\exp\left[-\frac{F}{RT}\left(E_{eq}-E_{cat/2}\right)\right] \quad \text{(Equation 5D)}$$

TOF_0 is analogous to the exchange current density (i.e., the magnitude of the equal oxidation and reduction currents that comprise the dynamic equilibrium at E_{eq}) obtained from extrapolating Tafel plots of heterogeneous materials to zero overpotential, and is proposed to represent the intrinsic catalytic properties of a molecular catalyst.[36]

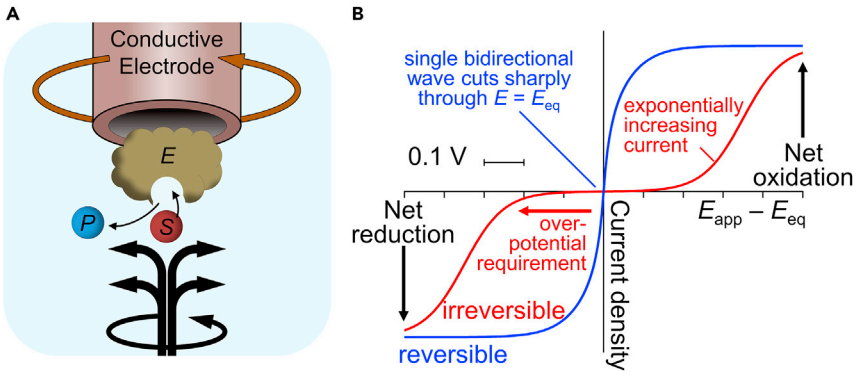

Figure 3. Overview of an electrocatalytic reaction involving an immobilized catalyst and a rotating electrode

(A) Depiction of an enzyme (*E*) immobilized onto a rotating conductive electrode surface. Chemical substrate (*S*) is continuously delivered to the electrode surface via forced convection, where it interacts with *E* to generate the product (*P*). The brown arrow represents rotation of the conductive electrode, and the black arrows represent the flow of electrolyte to the electrode surface.

(B) Steady-state electrochemical kinetics (Y axis) and thermodynamics (X axis) of reversible and irreversible processes visualized by voltammetry. The scale bar shows the potential range of 0.1 V. Although not shown in the figure, the anodic- versus cathodic-overpotential requirement can be biased toward favoring oxidation or reduction and thus differ in value for some enzymes. Likewise, the plateau anodic and cathodic currents can also vary in their absolute intensities.[44] Adapted with permission from Armstrong and Hirst.[45]

HETEROGENEOUS ELECTROCATALYSIS USING MOLECULAR COMPONENTS

Both redox enzymes and synthetic molecular electrocatalysts have been immobilized onto conductive supports for powering electrochemical transformations.[37–41] Although the electrocatalytic components of these assemblies are molecular in origin, the overall constructs are inherently heterogeneous. Still, the characteristic parameters used to benchmark homogeneous molecular electrocatalysts (e.g., K_M, k_{cat}, and $E_{cat/2}$) can be determined and used to benchmark hybrid, heterogenized assemblies.[36,42,43] Like their homogeneous counterparts, a description of the surface kinetics, including determinations of potential-independent rate constants, can be extracted from the limiting currents of S-shaped voltammograms. Such waveforms have been achieved using rotating electrode techniques, which avoid depleting the concentration of chemical substrates at the electrode surface by introducing a continuous flow of electrolyte solution (Figure 3A). In addition, stationary electrode techniques involving a relatively large excess of chemical substrate(s) and/or relatively high scan rates can yield experimental conditions where the limiting current becomes independent of the scan rate and no longer influenced by kinetics associated with diffusion of chemical substrates to the electrode surface.[42]

A theoretical framework for extracting the TOF of surface-confined catalysts, using information on the number of catalysts present on the electrode surface rather than in the reaction-diffusion layer, has been established by Savéant and coworkers.[36] In the case of redox enzymes immobilized on electrodes, protein film voltammetry has been utilized to extract thermodynamic and kinetic parameters.[46–49] Unlike more classical approaches to determining enzyme catalytic efficiency, which rely on the relationship between the concentration of reactants and their microscopic rates of binding, the rates of electrocatalytic reactions can also depend on the electrode potential. Thus, electrocatalytic enzymes add the potential dimension as an auxiliary experimental variable.[43]

Armstrong and Hirst note enzymes immobilized on rotating electrodes can be extremely efficient electrocatalysts,[45] meaning they display bidirectional voltammetric waves that switch sharply between net oxidation and reduction at the equilibrium potential (E_{eq}) associated with the redox half-reactions they catalyze, and achieve potential-independent limiting currents at relatively low overpotentials (Figure 3B). To extend the concepts of electrochemical reversibility and exchange current density to electrocatalysis by molecules attached to electrodes, the term electrocatalytic exchange current has been adopted.[44,45] It incorporates not only kinetics associated with interfacial electron transfer but also the turnover of the catalytic center and any intramolecular electron-transfer steps, each of which can limit the overall rate of electrocatalysis. In this approach, the electrocatalytic exchange current remains defined at E_{eq}. Thus, molecular electrocatalysts with relatively low electrocatalytic exchange currents and high overpotential requirements are defined as irreversible and inefficient. Conversely, electrocatalysts with relatively high electrocatalytic exchange currents and low anodic- and cathodic-overpotential requirements are defined as reversible and efficient. Reactions that are notoriously irreversible when driven by human-engineered catalysts, for example the reduction of CO_2, can be reversibly catalyzed using an appropriate enzyme. Such activity has been attributed to molecular evolution responding to stringent biological drivers for thermodynamic efficiency.[45] Enzymes thus set relatively high standards for activity and offer inspiration for designing reversible and efficient synthetic catalysts. However, their relatively large size and fragility limit their direct application in commercial technologies.[45]

Enzyme catalysis during protein film voltammetry measurements has been described using Michaelis-Menten-type kinetics under a rapid pre-equilibrium approximation, where all binding and unbinding steps are fast relative to chemical reactions within the *ES* complex.[43,50] For example, when electrode rotation rates are sufficiently high, the limiting currents for succinate oxidation by fumarate reductase are proportional to $\frac{k_2^{succ}[S]}{[S]+K_O^{succ}}$, where K_O^{succ} is the dissociation constant from the oxidized enzyme active site, and k_2^{succ} is the first-order rate constant for succinate oxidation in the *ES* complex. Thus, $K_O^{succ}$and k_2^{succ} can be determined from the limiting current measured under varying substrate concentration.

PHOTOELECTROSYNTHESIS AT MOLECULAR-ELECTROCATALYST-MODIFIED SEMICONDUCTORS

Elementary steps and rate laws describing semiconductor|liquid junction photoelectrochemistry, including charge-transfer reactions between semiconductor electrodes and electrolyte solutions containing redox-active agents that are not catalytic, have been previously described.[51–57] By contrast, relatively few models describing photoelectrosynthetic reactions involving molecular electrocatalysts immobilized on semiconductor electrodes have been presented,[19–25] and even fewer utilize experimental data to construct the related models. Nonetheless, molecular catalysts—including enzymes—are attractive for fundamental studies due to their well-defined structures that facilitate developing structure-activity relationships and advancing rational synthetic designs.[58,59]

A major difference between conducting and semiconducting electrodes is where the changes in potential appear following application of an external bias. Applying an external bias potential to a conducting electrode in contact with a liquid electrolyte results in a potential drop appearing mostly outside the electrode (i.e., across an electrical double layer in the liquid electrolyte), and increasing the bias increases

k_{et} in accordance with Marcus-Hush-Levich theory[30–32] and Butler-Volmer kinetics[33] (Figure 2). In contrast, applying an external bias potential to a semiconducting electrode in contact with a liquid electrolyte results in a potential drop appearing mostly inside the electrode (i.e., within the space-charge region), giving rise to changes in the degree of semiconductor valence- and conduction-band bending.[57,60] For an ideal n-type semiconducting electrode interfaced with a liquid electrolyte under illumination, oxidative polarization increases the degree of band bending within the space-charge region, thereby increasing the fraction of minority-carrier holes reaching the semiconductor surface. Conversely, for an ideal p-type semiconducting electrode interfaced with a liquid electrolyte under illumination, reductive polarization increases the degree of band bending within the space-charge region, thereby increasing the fraction of minority-carrier electrons reaching the semiconductor surface. Thus, for both materials (n-type and p-type) the dependence of the photocurrent density (a reaction rate) on the applied electrochemical bias (a thermodynamic driving force) is established by changing the concentration of charge carriers at the semiconductor|liquid interface, not the rate constant for charge transfer. However, under non-ideal conditions, where charge transfer and recombination are sluggish, a substantial concentration of carriers can build up at the surface of the semiconductor, causing a fraction of the potential drop to appear across the electrical double layer. This effect—known as Fermi level pinning and sometimes referred to as band edge unpinning—means the applied potential can, under non-ideal conditions, change the activation energy for interfacial charge transfer and hence the charge-transfer rate constants.[56,61]

Another significant difference between electrochemical reactions occurring at conducting electrodes versus photoelectrochemical reactions occurring at semiconducting electrodes is that charge-transfer reactions involving semiconductors can occur from conduction and valence bands. Illumination of a semiconductor in contact with an electrolyte results in formation of electron-hole pairs (e^--h^+). Once formed, the electron-hole pairs can separate into mobile charge carriers or recombine via nonradiative and radiative pathways.[62] In the case of an n-type semiconductor, the electric field inside the semiconductor drives minority-carrier holes in the valence band toward the liquid junction and majority-carrier electrons in the conduction band away from the liquid junction and toward an electrical contact. Conversely, in the case of a p-type semiconductor, the electric field inside the semiconductor drives minority-carrier electrons in the conduction band toward the liquid junction and majority-carrier holes in the valence band away from the liquid junction and toward an electrical contact. Kinetics associated with the transfer of valence-band holes across a semiconductor|liquid junction are governed by forward and reverse hole-transfer rate constants, whereas kinetics associated with the transfer of conduction-band electrons across a semiconductor|liquid junction are governed by forward and reverse electron-transfer rate constants. When the band bending is relatively high, the resulting electric field favors accumulation of minority carriers at the semiconductor|liquid interface while disfavoring the accumulation of majority carriers, and thereby significantly reducing the rates of their transfer. For perspective, the space-charge region within a semiconductor is on the order of hundreds of nanometers, and the resulting electric fields can be as high as 10^5 V cm^{-1}.[57]

The immobilization of molecular electrocatalysts onto semiconductor surfaces results in formation of semiconductor|catalyst interfaces. When these modified semiconductors are immersed in liquids, semiconductor|catalyst|liquid junctions are formed (Figures 4, 5, and 6). In general, molecular coatings are permeable to ions in electrolyte solutions, and the semiconductor|catalyst interfaces formed as a result

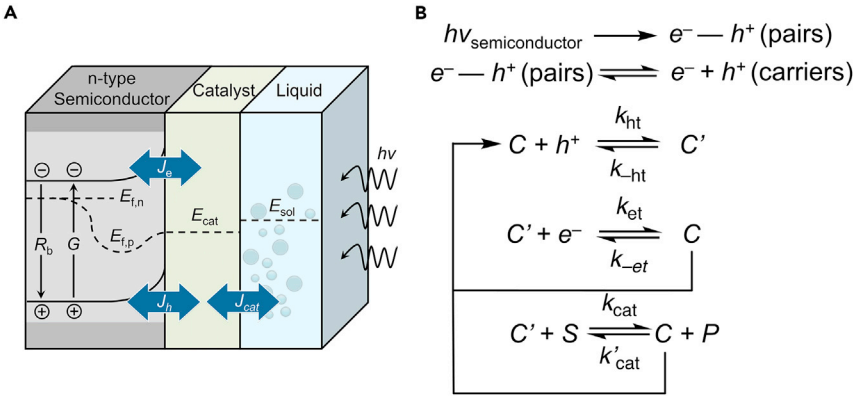

Figure 4. Example of a photoelectrosynthetic anode for oxygen evolution

(A) A schematic illustrating the anodic current density (J_h), cathodic current density (J_e), catalyst-solution current density (J_{cat}), rate of recombination (R_b), and rate of generation (G) associated with an electrocatalyst-modified n-type semiconductor in an aqueous solution under illumination. The quasi-Fermi levels for holes ($E_{f,p}$) and electrons ($E_{f,n}$) as well as the catalyst potential (E_{cat}) and solution potential (E_{sol}) are also indicated. Adapted with permission from Nellist et al.[20] Copyright 2016 American Chemical Society.

(B) A reaction scheme for photoelectrosynthesis at an n-type catalyst-modified semiconductor. Here, immobilized catalysts (C) are activated (forming C') via charge-transfer reactions involving surface holes and electrons, and the catalytic step is modeled as reversible. The relevant rate constants include k_{et}, k_{-et}, k_{ht}, k_{-ht}, k_{cat}, and k'_{cat} (see related text for further details).

of these coatings have been referred to as adaptive junctions.[20,21,63,64] Unlike more traditional Schottky-type buried junctions, where the catalyst potential tracks with changes in potential applied to the semiconductor electrode, in the case of adaptive junctions the permeability of ions permits the catalyst potential to move independently of the semiconductor potential and band edges.[20]

Current-potential responses predicted for molecular-electrocatalyst-modified n-type semiconductors that photoelectrosynthetically drive the oxygen-evolution reaction (Figure 4) have been modeled using a catalyst-solution current density (J_{cat}) and a semiconductor-catalyst current density (J_{jxn}) as shown in Equations 6A and 6B, respectively:[21]

$$J_{cat} = k_{cat}C' - k'_{cat}C = k_{cat}\widehat{C}\frac{e^{qV_{cat}/k_BT} - 1}{e^{qV_{cat}/k_BT} + K} \quad \text{(Equation 6A)}$$

$$J_{jxn} = J_h + J_e = \left(k_{ht}p_sC - k_{-ht}\{p_s\}C'\right) + \left(-k_{et}n_sC' + k_{-et}\{n_s\}C\right) \quad \text{(Equation 6B)}$$

In Equation 6A, J_{cat} is the current density between the catalyst and solution layers, k_{cat} and k'_{cat} are forward and reverse rate constants associated with chemical catalysis; $\widehat{C}$, C', and C are the concentrations of total, activated (i.e., oxidized form in the case of a photoanodic reaction), and non-activated (i.e., reduced form in the case of a photoanodic reaction) catalyst sites, respectively; qV_{cat} is the chemical potential difference across the catalyst layer; k_B is the Boltzmann constant; and K is the equilibrium constant for the reaction ($K = k_{cat}/k'_{cat}$). In Equation 6B, J_{jxn} is the current density between semiconductor and catalyst layers expressed as the sum of anodic (J_h) and cathodic (J_e) current densities, k_{ht} and k_{-ht} are the forward and reverse rate constants for hole transfer, k_{et} and k_{-et} are the forward and reverse rate constants for electron transfer, p_s and n_s are surface hole and electron concentrations, and $\{p_s\}$ and $\{n_s\}$ represent concentrations of unoccupied surface hole and electron states.

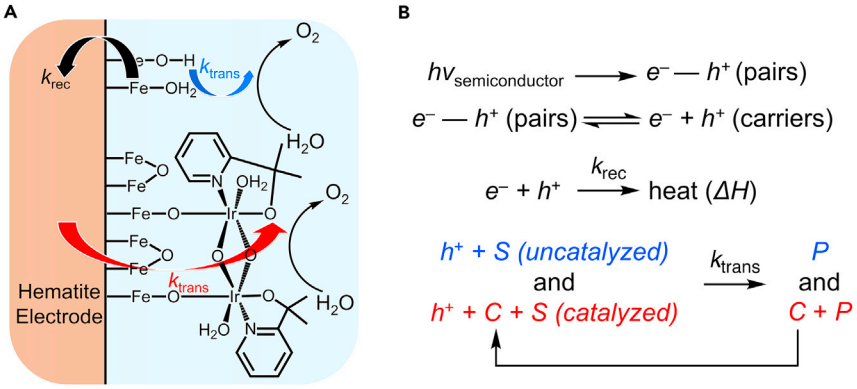

Figure 5. Example of a molecular-electrocatalyst-modified photoanode for oxygen evolution

(A) A schematic illustrating key kinetic parameters used to model the performance of hematite electrodes modified with a pseudo-molecular Ir catalyst. The rate constant of hole transfer from the surface to the solution (k_{trans}) and the rate constant associated with recombination of electrons with holes on the surface (k_{rec}) are indicated with arrows. Adapted with permission from Li et al.[23] Copyright 2016 The Royal Society of Chemistry.

(B) A reaction scheme for photoelectrosynthesis at an n-type catalyst-modified semiconductor. Here, photoelectrochemical fuel generation takes place either at surface states inherent to the semiconductor (i.e., uncatalyzed pathways) or through charge-transfer pathways involving surface-immobilized catalysts (i.e., catalyzed pathways). Overall charge-transfer efficiencies are described using the rate constants k_{rec} and k_{trans}.

When k_{cat} is relatively small and the applied potential is relatively large with respect to the open-circuit voltage, the concentration of surface-immobilized catalysts in their activated form, C', approaches the total concentration of surface-immobilized catalysts, $\widehat{C} = C' + C$. Under these conditions, the current is limited by the rate at which activated catalysts can oxidize the substrate. In contrast, when k_{cat} is relatively large, the current-potential response can be modeled using the current associated with the photodiode.[21] Results from this work indicate that semiconductor|catalyst interfaces featuring ion-permeable junctions can achieve higher photovoltages and efficiencies relative to semiconductors interfaced with dense layers of catalyst, because the maximum internal energy extracted from electron-hole pairs is variable. Such conclusions cannot be ascertained using traditional equivalent circuit models, but are central to the study and design of efficient photoelectrosynthetic assemblies.

In another example describing photoelectrosynthetic oxygen evolution (Figure 5), kinetic models were tested using intensity-modulated photocurrent spectroscopy and electrochemical impedance spectroscopy.[23] The authors compared the activities of unmodified, pseudo-molecular Ir catalyst-modified, and heterogeneous Ir oxide-modified hematite semiconductor electrodes by determining the rate constants associated with hole transfer from the surface to the solution (k_{trans}), the effective rate constants associated with recombination of electrons in the conduction band with holes on the surface (k_{rec}), and the overall hole-transfer efficiency (TE) determined using the values of k_{trans} and k_{rec} as shown in Equation 7:

$$TE = \frac{k_{trans}}{k_{trans} + k_{rec}} \quad \text{(Equation 7)}$$

The kinetic model used in this work was originally developed by Peter and coworkers to describe the photoelectrochemical behavior of hematite-based photocathodes.[65] It indicates the photocurrent density (J) and light intensity (I) should have

a linear relationship, where the slope of a *J-I* plot yields the external quantum efficiency of the photoelectrochemical processes.[66] As noted by the authors, the following assumptions are made regarding this kinetic model: (1) water oxidation by hematite is mediated by surface states, including electronic states induced by surface chemisorption;[67–69] (2) hole transfer from the valence band of hematite to the surface states is fast, not rate limiting, and thus not considered in the model;[70] (3) the rate at which holes transfer from the surface to the solution is pseudo-first-order with respect to the concentration of holes on the surface;[23] and (4) the rate at which electrons recombine with holes on the surface is first order with respect to the concentration of holes on the surface.[66,71]

Significantly higher values of k_{trans} were measured using hematite electrodes modified with either the pseudo-molecular Ir catalysts or heterogeneous Ir oxide. For example, the highest value of k_{trans} measured using unmodified hematite electrodes was 57.09 $\pm$ 21.27 s^{-1} at E_{app} = 1.3 V versus the reversible hydrogen electrode (RHE) potential, whereas the highest value of k_{trans} measured using pseudo-molecular Ir catalyst-modified and heterogeneous Ir oxide-modified hematite electrodes were 140.65 $\pm$ 1.26 s^{-1} at E_{app} = 1.2 V versus RHE and 146.44 $\pm$ 16.08 s^{-1} at 0.8 V versus RHE, respectively. However, a key difference between the surface coatings is observed when comparing values of k_{rec}. The values of k_{rec} recorded following application of the pseudo-molecular Ir catalysts remain relatively unchanged, whereas the values of k_{rec} recorded following application of the heterogeneous Ir oxide are significantly lower. For example, at E_{app} = 0.8 V versus RHE, k_{rec} values of 187.56 $\pm$ 32.61 s^{-1}, 208.60 $\pm$ 10.70 s^{-1}, and 65.45 $\pm$ 0.40 s^{-1} were recorded using the unmodified, pseudo-molecular Ir catalyst-modified, and heterogeneous Ir oxide-modified hematite electrodes, respectively. These results indicate the heterogeneous Ir oxide catalyst film replaces the hematite|H_2O interface with one that is fundamentally different. This work also provides a systematic approach for comparing values of the rate constants k_{trans} and k_{rec}, which determine the transfer efficiency.

Experimental results using molecular-electrocatalyst-modified p-type gallium phosphide electrodes containing cobalt porphyrin hydrogen evolution reaction electrocatalysts (Figure 6A) have also been used to construct conceptual frameworks and rate laws relevant to photoelectrosynthesis.[22] In these efforts, current-potential responses of the molecular-electrocatalyst-modified semiconductors (Equation 8A) were modeled by applying either steady-state (Equation 8B) or rapid pre-equilibrium (Equation 8C) approximations to describe the fraction of surface-immobilized catalysts present in their activated form under varying bias potentials, scan rates, pH conditions, and intensities of simulated solar illumination. The elementary photoelectrochemical reaction steps shown in Figure 6B, where the catalytic step is governed by the rate constant k_{cat} and is an irreversible step, were used to construct these rate laws, yielding expressions similar in mathematical form to those appearing in the Michaelis-Menten model:

$$J = \frac{nF}{FE} * k_{cat}\Gamma_{C'} \qquad \text{(Equation 8A)}$$

$$J = \frac{nF}{FE} * \frac{k_{cat}\,\Gamma_{C_T} n_s}{\frac{k_{-et}+k_{cat}}{k_{et}} + n_s} \qquad \text{(Equation 8B)}$$

$$J = \frac{nF}{FE} * \frac{k_{cat}\,\Gamma_{C_T} n_s}{K^{-1} + n_s} \qquad \text{(Equation 8C)}$$

In these equations, J is the current density, n is the number of electrons required for the chemical transformation, F is the Faraday constant, FE is the faradaic efficiency,

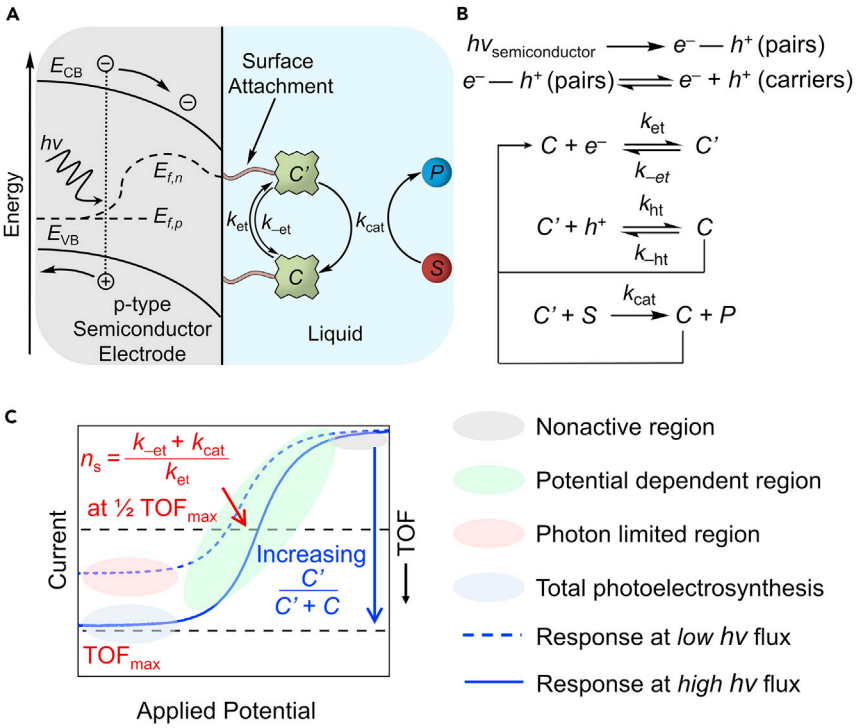

Figure 6. Example of a photoelectrosynthetic cathode for hydrogen evolution

(A) A Gerischer-type energy versus distance diagram involving a molecular-electrocatalyst-modified p-type semiconductor in a liquid solution. Under illumination, photons are absorbed by the semiconductor, exciting electrons from the valence band (E_{VB}) to the conduction band (E_{CB}), resulting in a splitting of the Fermi level into the electron quasi-Fermi level ($E_{f,n}$) and hole quasi-Fermi level ($E_{f,p}$). Electrons driven to the semiconductor|liquid interface are transferred to the surface-immobilized catalysts (C) to form the activated catalyst species (C'), where k_{et} and k_{-et} represent the forward and reverse electron-transfer rate constants between the semiconductor surface and immobilized catalysts. Once formed, C' can react with chemical substrate (S) to form the product (P) and regenerate C with kinetics governed by the potential-independent rate constant for catalysis (k_{cat}).

(B) A reaction scheme for photoelectrosynthesis.

(C) A plot of the current produced by a photoelectrosynthetic reaction versus the applied potential at either relatively low (dashed blue) or high (solid blue) light flux. Points along the voltammograms associated with TOF_{max} and the surface concentration of electrons required to achieve $\frac{1}{2}$ TOF_{max} ($\frac{k_{-et}+k_{cat}}{k_{et}}$) are indicated with dashed black lines.

k_{cat} is a pseudo-first-order rate constant, k_{et} and k_{-et} are the forward and reverse rate constants for electron transfer between the semiconductor and catalyst layer, respectively, $\Gamma_{C'}$ and Γ_{C_T} are the per geometric area surface density of activated and total catalysts, respectively, n_s represents the surface electron concentration under steady-state illumination, and K^{-1} is an equilibrium constant equal to the ratio k_{-et}/k_{et}.

Using this approach, distinct regions of the voltammogram waveforms were identified and related to the relative concentration of activated catalysts on the electrode surfaces (Figure 6C). In the nonactive region, where the working electrode is polarized at potentials positive of the open-circuit voltage under illumination, the fraction of activated catalyst is near zero and the current density response and related rate of chemical product formation do not change significantly as the applied potential is adjusted within this region. In the potential-dependent region, where the working electrode is polarized at potentials negative of the open-circuit voltage, increasing

the applied bias potential increases the fraction of minority-carrier electrons reaching the semiconductor surface, and thus increases the steady-state concentration of activated catalysts. In this region, the limiting current density is expressed using a steady-state approximation (Equation 8B). Under relatively low light fluxes and upon applying a sufficiently negative bias potential, the current density response of the illuminated working electrodes reaches limiting values that are potential independent but proportional to the intensity of the illumination. In this photon-limited region, the limiting current density is again expressed using a steady-state approximation, but the electrode is now photon starved. Thus, the steady-state concentrations of surface electrons and activated catalysts become independent of the bias potential and degree of band bending. Finally, a region where the current density is potential independent and no longer limited by photon flux, termed the total photoelectrosynthesis region, is proposed. In this region, the fraction of catalysts at the electrode surface in their activated form is near unity, and the limiting current density is expressed using a rapid pre-equilibrium approximation (Equation 8C). Although distinct regions of the voltammograms in Figure 6C are indicated for simplicity, in practice a transition from the photon-limited region to the total photoelectrosynthesis region would be continuous and likely include a region where both steady-state and pre-equilibrium approximations can be applied.[72]

As previously mentioned, the term K_M—as used in the Michaelis-Menten model when applying a steady-state approximation—is equal to $\frac{k_r + k_{cat}}{k_f}$, and it defines the initial concentration of chemical substrate required to achieve half the maximum velocity of an enzyme. In the photoelectrosynthetic model, the related term $\frac{k_{-et} + k_{cat}}{k_{et}}$ from Equation 8B represents the electron surface concentration—not the concentration of chemical substrate—required to activate one-half of the immobilized catalysts. In this context, $\frac{k_{-et} + k_{cat}}{k_{et}}$ can also be viewed as a photoelectrochemical counterpart of the electrocatalytic half-wave potential, $E_{cat/2}$. As previously mentioned, $E_{cat/2}$ is the electrocatalytic benchmarking parameter indicating the potential required to activate half the catalysts at the electrode surface and thus achieve half the maximum electrocatalytic activity. In a related manner, Equation 8C is similar in form to rate laws associated with Michaelis-Menten enzyme-substrate kinetics when applying a rapid pre-equilibrium approximation. The constant K^{-1}, which is equal to the ratio k_{-et}/k_{et}, can be viewed as the photoelectrochemical counterpart of the Michaelis-Menten dissociation constant, K_d, which is equal to k_r/k_f and is the thermodynamic parameter quantifying the equilibrium between the enzyme in its substrate-bound (*ES*) and -unbound (*E*) forms.

If the photoelectrosynthetic illumination intensity, value of k_{et}, and concentration of chemical substrates, are sufficiently high, n_s would approach a value required to activate all catalysts upon sufficiently biasing the electrode potential, and the current would become limited by the TOF_{max} of the catalysts. However, such conditions have yet to be achieved experimentally, and only conditions where the saturating currents are limited by the flux of photons were observed in these studies. For context, the total photon flux obtained via integration of the air mass (AM) 1.5 global tilt solar spectrum from 280 to 4,000 nm is 4.3×10^{17} s^{-1} cm^{-2}. If a catalyst-modified photoelectrode utilized this flux with unity external quantum efficiency across all wavelengths, it would operate at a current density of 69 mA cm^{-2}. At a per geometric area catalyst loading of 1 nmol cm^{-2}, the related per catalyst TOF for driving a two-electron half-reaction such as hydrogen evolution would be 358 s^{-1}.

Although Equations 8A, 8B, and 8C account only for minority-carrier currents, these equations have been extended to account for majority-carrier currents.[22] The

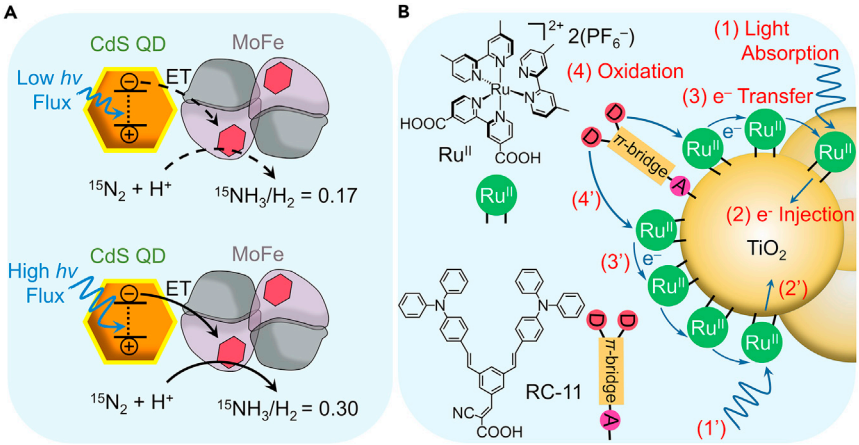

Figure 7. Examples of materials for light-activated nitrogen reduction and the accumulation of redox equivalents

(A) A schematic indicating the reduction of nitrogen to ammonia by complexes of nitrogenase MoFe protein and CdS QDs. The selectivity of the complex for ammonia production is dependent on the rate of photoexcited electron injection into the MoFe protein, which depends on the light flux. Adapted with permission from Brown et al.[25] (https://pubs.acs.org/doi/10.1021/acscatal.0c02933). Copyright 2020 American Chemical Society (ACS). Further permissions related to the material excerpted should be directed to the ACS.

(B) A schematic indicating the sequence of steps proposed for accumulating two oxidation equivalents on a proxy for a molecular catalyst (RC-11) immobilized onto dye-sensitized TiO_2 particles, including light absorption by the dye molecules (Ru^{II}) (steps 1 and 1′), excited-state electron injection into the TiO_2 particles to form Ru^{III} (steps 2 and 2′), self-exchange electron transfer between immobilized Ru dyes (steps 3 and 3′), and $[RC\text{-}11]^0$ being twice oxidized to form $[RC\text{-}11]^{2+}$ (steps 4 and 4′). Adapted with permission from Chen and Ardo.[81] Copyright 2018 Springer Nature.

approximation of considering only minority-carrier currents is similar to that used in the Gärtner model[73] and, like the Gärtner model, which represents an upper limit for the photocurrent response of a semiconductor, would deviate from experimental results under conditions giving rise to relatively low band bending and high rates of charge recombination.[55]

In addition to photoelectrochemical assemblies featuring human-engineered catalysts, there has been significant progress in developing semi-natural biohybrid assemblies, including photoelectrochemical cells interfaced with photosystem I and/or photosystem II complexes of oxygen-evolving photosynthetic organisms as well as photoelectrochemical cells interfaced with purple bacterial reaction centers.[74–79] Some of these assemblies display illumination-intensity-independent photocurrent responses.[76] However, in these cases, extracting benchmarking parameters relevant to chemical catalysis at an active site can be complicated by rate-limiting steps associated with the binding/unbinding of chemical substrates. As an example, the 50 s^{-1} TOF associated with the oxygen-evolving complex (OEC) of photosystem II is not a maximum TOF or a catalytic rate constant inherent to the OEC; rather, it is a value limited by diffusion of quinones into and out of the secondary quinone (Q_B) binding site.[80]

A modified version of the Michaelis-Menten equation was used to characterize the nitrogen reduction versus hydrogen evolution activities of complexes formed from nitrogenase MoFe proteins and CdS quantum dots (CdS QDs) (Figure 7A).[25] To quantify the effect of light intensity on the photoelectrochemical activity, TOFs

associated with ammonia and hydrogen production were fitted separately using Equation 9:

$$V = \frac{V_{max} * S}{S + K_{1/2}} \quad \text{(Equation 9)}$$

where S is the concentration of total photons absorbed, and $K_{1/2}$ is the concentration of absorbed photons necessary to achieve $\frac{1}{2} V_{max}$. In this equation, the S and $K_{1/2}$ terms replace the n_s and $\frac{k_{-et} + k_{cat}}{k_{et}}$ terms used in Equation 8B. Thus, Equation 9 is expressed in terms of the photon concentration required to achieve half the maximum activity rather than the related minority-carrier surface concentration as expressed in Equation 8B. As pointed out by the authors, S is proportional to the light intensity, and changing the light intensity changes the concentration of substrate electrons available to catalytic sites over the course of the reaction.

Results from this work show that adjusting the light intensity alters the ratio of ammonia versus hydrogen generated as chemical products. At relatively low light intensities (from 11 to 26 mM of total photons absorbed per reaction volume), and thus low excitation rates, the electron-transfer rate to the MoFe protein from the CdS QDs limits the accumulation of four electrons at the MoFe-cofactor site. These conditions result in a relatively low TOF for the six-electron nitrogen reduction reaction and instead favor the two-electron hydrogen evolution chemistry with $^{15}NH_3/H_2$ ratios as low as 0.17. Conversely, at relatively high light intensities (from 45 to 138 mM of total photons absorbed per reaction volume), and thus high excitation rates, the enhanced rates of electron transfer yield improved TOFs for nitrogen reduction and achieve $^{15}NH_3/H_2$ ratios that approach ~0.30. This work establishes an approach for using illumination intensities and rates of photoexcitation to control the product distribution of multi-electron, multi-proton reactions relevant to solar photochemistry.[24,82,83]

In the context of accumulating multiple redox equivalents at catalytically active sites, studies involving light-activated assemblies featuring TiO_2 particles functionalized with a molecular dye (a ruthenium-based chromophore abbreviated as Ru^{II}; see Figure 7B) and a proxy for a molecular catalyst (a bistriphenylamine-based complex abbreviated as RC-11; see Figure 7B) indicate optimization of catalyst loading plays an important role.[81,84] In particular, relatively low surface loadings of RC-11 (ranging from 1% to 3% of the total number of surface-anchored molecules and as compared with experiments performed at relatively high loading of 28% to 97% of the total number of surface-anchored molecules) were shown to favor accumulation of two redox equivalents at a single redox-active site, and mitigate parasitic light absorption by the catalytic layer.[85–88] This less-is-more strategy is in contrast to a more common approach taken in electrocatalysis, where maximizing the electrode surface area and loading of active catalysts is used to achieve higher activities. Thus, this work showcases the importance of utilizing catalyst with relatively high TOF_{max} values rather than relying on a higher loading of catalyst with relatively lower TOF_{max} values and similar $E_{cat/2}$ values. Still, even in the case of electrocatalytic assemblies, both experimental and theoretical results show that excessively thick loadings can become detrimental to the overall, average catalytic TOF if the loadings are so thick that charges cannot be effectively transferred from the underlying electrode, or if the required chemical substrates cannot reach electroactive sites within the film.[89–92]

Parameters and rate laws used to characterize the performance of enzymes, molecular electrocatalysts, and light-activated assemblies are summarized in Table 1. These selections showcase examples where reaction activity is modeled using a

Table 1. Examples of rate laws and TOF expressions used to characterize enzymatic, electrocatalytic, photoelectrosynthetic, and photochemical reactions

Classes	Concentration-related constants	Kinetic parameters	Related rate laws and TOF expressions
Enzymatic[9–11]	K_M	$V_{max} = k_{cat}[E]_0$	$v = \frac{V_{max}[S]}{K_M + [S]}$
Electrocatalytic[12,13]	$E_{cat/2}$	$TOF_{max} = k_{cat}$	$TOF = \frac{TOF_{max}}{1 + \exp\left[\frac{RT}{F}(E_{app} - E_{cat/2})\right]}$
Photoelectrosynthetic[22]	$\frac{k_{-et} + k_{cat}}{k_{et}}$	$TOF_{max} = k_{cat}$	$J = \frac{nF}{FE} * \frac{k_{cat}\Gamma_{C_T} n_s}{\frac{k_{-et} + k_{cat}}{k_{et}} + n_s}$
Photochemical[25]	$K_{1/2}$	V_{max}	$v = \frac{V_{max} S}{K_{1/2} + S}$

In enzymatic catalysis, the Michaelis constant (K_M) defines the concentration of chemical substrate required for an enzyme to function at half its maximum velocity ($\frac{1}{2}$ V_{max}). In molecular electrocatalysis (synthetic or biological), $E_{cat/2}$ represents the applied bias potential required to activate half the catalysts within the reaction-diffusion layer, and TOF_{max} is the per catalytic site maximum turnover frequency. In photoelectrosynthetic assemblies featuring synthetic molecular catalysts and semiconductor electrodes, the constant $\frac{k_{-et} + k_{cat}}{k_{et}}$ has been used to represent the electron surface concentration required to activate half the catalysts immobilized on a light-absorbing semiconductor surface. In a related vein, the term $K_{1/2}$ has been used to represent the concentration of photons required to achieve $\frac{1}{2}$ V_{max} for photochemical assemblies featuring semiconductor and enzyme complexes.

kinetic descriptor and a constant expressing the electrode potential or concentration of reactants (i.e., chemical substrates, electrons, or photons) required to achieve half the maximum activity. The light-activated assemblies featured in this perspective utilize varying light-capture materials (e.g., bulk n-type semiconductors, bulk p-type semiconductors, quantum dots, or dye-sensitized nanoparticles), and contrast in their use of molecular components (e.g., enzymes, synthetic molecular catalysts, or proxies for molecular catalysts) for driving varying synthetic transformations (e.g., oxygen evolution, hydrogen evolution, or nitrogen reduction). Despite their differences, all of the light-activated constructs use photons as a reagent, offering opportunities to better understand and ultimately control how charge carriers move through these diverse materials under varying operating conditions.

CONCLUSION AND OUTLOOK

Methods for determining enzyme catalytic efficiency and the benchmarking of molecular electrocatalysts provide strategies for identifying characteristics that limit their performance. These efforts have advanced the rational synthesis of artificial enzymes[93–96] and electrocatalytic assemblies.[14,37,97] Related analyses of emerging molecular-electrocatalyst-modified semiconductors involving interactions with light have not been as rigorously developed. Unlike metals, where the concentration of surface electrons can be relatively high, the concentration of charge carriers at semiconductor surfaces can become limiting under relatively low light intensities, and their conduction/valence-band character versus surface-state character can be unclear. Although treating electrons and photons as reaction partners makes it possible to derive frameworks for extracting kinetic and thermodynamic figures of merit, the binding of chemical components is physically different from transferring charge carriers between (semi)conducting solid surfaces and electrocatalytic components. Electrons and photons are probabilistic in nature. In contrast, enzymes, synthetic molecular catalysts, and chemical substrates have more well-defined and localized structures.

The examples highlighted in this perspective set the stage for better understanding parallels and differences of catalysis across biological and technological ensembles. However, there is currently not enough understanding of how charge carriers move through these diverse materials to provide a complete picture of rational design principles. Comparisons of results are further complicated by differences in experimental conditions and/or assumptions used in modeling of the data, including deviation from any assumed ideal conditions. In conclusion, further theory, computational, and experimental results are needed to improve and/or validate existing models. This perspective aims to bridge concepts, nomenclature, and benchmarking techniques used across different research communities studying catalysis, while also highlighting key differences, assumptions, and limitations.

ACKNOWLEDGMENTS

This work was supported by the National Science Foundation under Early Career Award 1653982 (materials and synthesis) and by the US Department of Energy, Office of Science, Office of Basic Energy Sciences, under Early Career Award DE-SC0021186 (modeling and benchmarking). G.F.M. acknowledges support from the Camille Dreyfus Teacher-Scholar Awards Program. B.L.W. was supported by an IGERT-SUN fellowship, funded by the National Science Foundation (1144616), and the Phoenix Chapter of the ARCS Foundation.

AUTHOR CONTRIBUTIONS

D.N., B.L.W., and G.F.M. researched the concepts and wrote the manuscript. D.N. and B.L.W. contributed equally.

DECLARATION OF INTERESTS

The authors declare no competing interests.

REFERENCES

1. Faunce, T., Styring, S., Wasielewski, M.R., Brudvig, G.W., Rutherford, A.W., Messinger, J., Lee, A.F., Hill, C.L., Degroot, H., Fontecave, M., et al. (2013). Artificial photosynthesis as a frontier technology for energy sustainability. Energy Environ. Sci. *6*, 1074–1076.

2. Ardo, S., Fernandez Rivas, D., Modestino, M.A., Schulze Greiving, V., Abdi, F.F., Alarcon Llado, E., Artero, V., Ayers, K., Battaglia, C., Becker, J.P., et al. (2018). Pathways to electrochemical solar-hydrogen technologies. Energy Environ. Sci. *11*, 2768–2783.

3. Bard, A.J., and Fox, M.A. (1995). Artificial photosynthesis: solar splitting of water to hydrogen and oxygen. Acc. Chem. Res. *28*, 141–145.

4. Zhang, B., and Sun, L. (2019). Artificial photosynthesis: opportunities and challenges of molecular catalysts. Chem. Soc. Rev. *48*, 2216–2264.

5. Andreiadis, E.S., Chavarot-Kerlidou, M., Fontecave, M., and Artero, V. (2011). Artificial photosynthesis: from molecular catalysts for light-driven water splitting to photoelectrochemical cells. Photochem. Photobiol. *87*, 946–964.

6. Cedeno, D., Krawicz, A., and Moore, G.F. (2015). Hybrid photocathodes for solar fuel production: coupling molecular fuel-production catalysts with solid-state light harvesting and conversion technologies. Interface Focus *5*, 20140085.

7. Dalle, K.E., Warnan, J., Leung, J.J., Reuillard, B., Karmel, I.S., and Reisner, E. (2019). Electro- and solar-driven fuel synthesis with first row transition metal complexes. Chem. Rev. *119*, 2752–2875.

8. Laidler, K.J. (1996). A glossary of terms used in chemical kinetics, including reaction dynamics (IUPAC Recommendations 1996). Pure Appl. Chem. *68*, 149–192.

9. Michaelis, L., and Menten, M. (1913). Die Kinetik der Invertinwirkung. Biochem. Z. *49*, 333–369.

10. Johnson, K.A., and Goody, R.S. (2011). The original Michaelis constant: translation of the 1913 Michaelis–Menten paper. Biochemistry *50*, 8264–8269.

11. Briggs, G.E., and Haldane, J.B.S. (1925). A note on the kinetics of enzyme action. Biochem. J. *19*, 338–339.

12. Artero, V., and Savéant, J.-M. (2014). Toward the rational benchmarking of homogeneous H_2-evolving catalysts. Energy Environ. Sci. *7*, 3808–3814.

13. Costentin, C., and Savéant, J.-M. (2017). Towards an intelligent design of molecular electrocatalysts. Nat. Rev. Chem. *1*, 87.

14. Lee, K.J., Elgrishi, N., Kandemir, B., and Dempsey, J.L. (2017). Electrochemical and spectroscopic methods for evaluating molecular electrocatalysts. Nat. Rev. Chem. *1*, 0039.

15. Rountree, E.S., McCarthy, B.D., Eisenhart, T.T., and Dempsey, J.L. (2014). Evaluation of homogeneous electrocatalysts by cyclic voltammetry. Inorg. Chem. *53*, 9983–10002.

16. Appel, A.M., and Helm, M.L. (2014). Determining the overpotential for a molecular electrocatalyst. ACS Catal. *4*, 630–633.

17. Sucheta, A., Cammack, R., Weiner, J., and Armstrong, F.A. (1993). Reversible electrochemistry of fumarate reductase immobilized on an electrode surface. Direct voltammetric observations of redox centers and their participation in rapid catalytic electron transport. Biochemistry *32*, 5455–5465.

18. Costentin, C., and Savéant, J.-M. (2014). Multielectron, multistep molecular catalysis of electrochemical reactions: benchmarking of homogeneous catalysts. ChemElectroChem *1*, 1226–1236.

19. Sathrum, A.J., and Kubiak, C.P. (2011). Kinetics and limiting current densities of homogeneous and heterogeneous electrocatalysts. J. Phys. Chem. Lett. *2*, 2372–2379.

20. Nellist, M.R., Laskowski, F.A.L., Lin, F., Mills, T.J., and Boettcher, S.W. (2016). Semiconductor–electrocatalyst interfaces: theory, experiment, and applications in photoelectrochemical water splitting. Acc. Chem. Res. *49*, 733–740.

21. Mills, T.J., Lin, F., and Boettcher, S.W. (2014). Theory and simulations of electrocatalyst-coated semiconductor electrodes for solar water splitting. Phys. Rev. Lett. *112*, 1–5.

22. Wadsworth, B.L., Beiler, A.M., Khusnutdinova, D., Reyes Cruz, E.A., and Moore, G.F. (2019). Interplay between light flux, quantum efficiency, and turnover frequency in molecular-modified photoelectrosynthetic assemblies. J. Am. Chem. Soc. *141*, 15932–15941.

23. Li, W., He, D., Sheehan, S.W., He, Y., Thorne, J.E., Yao, X., Brudvig, G.W., and Wang, D. (2016). Comparison of heterogenized molecular and heterogeneous oxide catalysts for photoelectrochemical water oxidation. Energy Environ. Sci. *9*, 1794–1802.

24. Brown, K.A., Harris, D.F., Wilker, M.B., Rasmussen, A., Khadka, N., Hamby, H., Keable, S., Dukovic, G., Peters, J.W., Seefeldt, L.C., et al. (2016). Light-driven dinitrogen reduction catalyzed by a CdS:nitrogenase MoFe protein biohybrid. Science *352*, 448–450.

25. Brown, K.A., Ruzicka, J., Kallas, H., Chica, B., Mulder, D.W., Peters, J.W., Seefeldt, L.C., Dukovic, G., and King, P.W. (2020). Excitation-rate determines product stoichiometry in photochemical ammonia production by CdS quantum dot-nitrogenase MoFe protein complexes. ACS Catal. *10*, 11147–11152.

26. Henri, V. (1903). Lois générales de l'action des diastases. Nature *68*, 221.

27. Miyanaga, K., and Unno, H. (2011). Reaction kinetics and stoichiometry. In Comprehensive Biotechnology, 2nd Edition, M. Moo-Young, ed. (Elsevier B.V.), pp. 33–46.

28. Albery, W.J., and Knowles, J.R. (1976). Evolution of enzyme function and the development of catalytic efficiency. Biochemistry *15*, 5631–5640.

29. Eisenthal, R., Danson, M.J., and Hough, D.W. (2007). Catalytic efficiency and k_{cat}/K_M: a useful comparator? Trends Biotechnol. *25*, 247–249.

30. Henstridge, M.C., Laborda, E., Rees, N.V., and Compton, R.G. (2012). Marcus-Hush-Chidsey theory of electron transfer applied to voltammetry: a review. Electrochim. Acta *84*, 12–20.

31. Marcus, R.A. (1965). On the theory of electron-transfer reactions. VI. Unified treatment for homogeneous and electrode reactions. J. Chem. Phys. *43*, 679–701.

32. Hush, N.S. (1958). Adiabatic rate processes at electrodes. I. Energy-Charge relationships. J. Chem. Phys. *28*, 962–972.

33. Bard, A.J., and Faulkner, L.R. (2001). Electrochemical Methods: Fundamentals and Applications, 2nd Edition (Wiley & Sons).

34. Khusnutdinova, D., Wadsworth, B.L., Flores, M., Beiler, A.M., Reyes Cruz, E.A., Zenkov, Y., and Moore, G.F. (2018). Electrocatalytic properties of binuclear Cu(II) fused porphyrins for hydrogen evolution. ACS Catal. *8*, 9888–9898.

35. Rountree, E.S., Martin, D.J., McCarthy, B.D., and Dempsey, J.L. (2016). Linear free energy relationships in the hydrogen evolution reaction: kinetic analysis of a cobaloxime catalyst. ACS Catal. *6*, 3326–3335.

36. Costentin, C., Drouet, S., Robert, M., and Savéant, J.-M. (2012). Turnover numbers, turnover frequencies, and overpotential in molecular catalysis of electrochemical reactions. Cyclic voltammetry and preparative-scale electrolysis. J. Am. Chem. Soc. *134*, 11235–11242.

37. Bullock, R.M., Das, A.K., and Appel, A.M. (2017). Surface immobilization of molecular electrocatalysts for energy conversion. Chem. Eur. J. *23*, 7626–7641.

38. Armstrong, F.A., Belsey, N.A., Cracknell, J.A., Goldet, G., Parkin, A., Reisner, E., Vincent, K.A., and Wait, A.F. (2009). Dynamic electrochemical investigations of hydrogen oxidation and production by enzymes and implications for future technology. Chem. Soc. Rev. *38*, 36–51.

39. Coutard, N., Kaeffer, N., and Artero, V. (2016). Molecular engineered nanomaterials for catalytic hydrogen evolution and oxidation. Chem. Commun. *52*, 13728–13748.

40. King, P.W. (2013). Designing interfaces of hydrogenase–nanomaterial hybrids for efficient solar conversion. Biochim. Biophys. Acta Bioenerg. *1827*, 949–957.

41. Wadsworth, B.L., Khusnutdinova, D., and Moore, G.F. (2018). Polymeric coatings for applications in electrocatalytic and photoelectrosynthetic fuel production. J. Mater. Chem. A *6*, 21654–21665.

42. Limoges, B., Moiroux, J., and Savéant, J.-M. (2002). Kinetic control by the substrate and the cosubstrate in electrochemically monitored redox enzymatic immobilized systems. Catalytic responses in cyclic voltammetry and steady state techniques. J. Electroanal. Chem. *521*, 8–15.

43. Léger, C., Heffron, K., Pershad, H.R., Maklashina, E., Luna-Chavez, C., Cecchini, G., Ackrell, B.A.C., and Armstrong, F.A. (2001). Enzyme electrokinetics: energetics of succinate oxidation by fumarate reductase and succinate dehydrogenase. Biochemistry *40*, 11234–11245.

44. Pandey, K., Islam, S.T.A., Happe, T., and Armstrong, F.A. (2017). Frequency and potential dependence of reversible electrocatalytic hydrogen interconversion by [FeFe]-hydrogenases. Proc. Natl. Acad. Sci. U S A *114*, 3843–3848.

45. Armstrong, F.A., and Hirst, J. (2011). Reversibility and efficiency in electrocatalytic energy conversion and lessons from enzymes. Proc. Natl. Acad. Sci. U S A *108*, 14049–14054.

46. Armstrong, F.A., Heering, H.A., and Hirst, J. (1997). Reaction of complex metalloproteins studied by protein-film voltammetry. Chem. Soc. Rev. *26*, 169–179.

47. Léger, C., Elliott, S.J., Hoke, K.R., Jeuken, L.J.C., Jones, A.K., and Armstrong, F.A. (2003). Enzyme electrokinetics: using protein film voltammetry to investigate redox enzymes and their mechanisms. Biochemistry *42*, 8653–8662.

48. Hirst, J. (2006). Elucidating the mechanisms of coupled electron transfer and catalytic reactions by protein film voltammetry. Biochim. Biophys. Acta Bioenerg. *1757*, 225–239.

49. Gulaboski, R., Mirčeski, V., Bogeski, I., and Hoth, M. (2012). Protein film voltammetry: electrochemical enzymatic spectroscopy. A review on recent progress. J. Solid State Electrochem. *16*, 2315–2328.

50. Léger, C., Dementin, S., Bertrand, P., Rousset, M., and Guigliarelli, B. (2004). Inhibition and aerobic inactivation kinetics of *Desulfovibrio fructosovorans* NiFe hydrogenase studied by protein film voltammetry. J. Am. Chem. Soc. *126*, 12162–12172.

51. Gerischer, H. (1969). Charge transfer processes at semiconductor-electrolyte interfaces in connection with problems of catalysis. Surf. Sci. *18*, 97–122.

52. Gerischer, H. (1991). Electron-transfer kinetics of redox reactions at the semiconductor/electrolyte contact. A new approach. J. Phys. Chem. *95*, 1356–1359.

53. Lewis, N.S. (1991). An analysis of charge transfer rate constants for semiconductor/liquid interfaces. Annu. Rev. Phys. Chem. *42*, 543–580.

54. Nozik, A.J., and Memming, R. (1996). Physical chemistry of semiconductor–liquid interfaces. J. Phys. Chem. *100*, 13061–13078.

55. Peter, L.M. (1990). Dynamic aspects of semiconductor photoelectrochemistry. Chem. Rev. *90*, 753–769.

56. Bard, A.J., Bocarsly, A.B., Fan, F.R.F., Walton, E.G., and Wrighton, M.S. (1980). The concept of Fermi level pinning at semiconductor/liquid junctions. Consequences for energy conversion efficiency and selection of useful solution redox couples in solar devices. J. Am. Chem. Soc. *102*, 3671–3677.

57. Walter, M.G., Warren, E.L., McKone, J.R., Boettcher, S.W., Mi, Q., Santori, E.A., and Lewis, N.S. (2010). Solar water splitting cells. Chem. Rev. *110*, 6446–6473.

58. Corbin, N., Zeng, J., Williams, K., and Manthiram, K. (2019). Heterogeneous molecular catalysts for electrocatalytic CO_2 reduction. Nano Res. *12*, 2093–2125.

59. McKone, J.R., Marinescu, S.C., Brunschwig, B.S., Winkler, J.R., and Gray, H.B. (2014). Earth-abundant hydrogen evolution electrocatalysts. Chem. Sci. *5*, 865–878.

60. Zhang, Z., and Yates, J.T. (2012). Band bending in semiconductors: chemical and physical consequences at surfaces and interfaces. Chem. Rev. *112*, 5520–5551.

61. Peter, L.M. (2013). Energetics and kinetics of light-driven oxygen evolution at semiconductor electrodes: the example of hematite. J. Solid State Electrochem. *17*, 315–326.

62. Würfel, U., Cuevas, A., and Würfel, P. (2015). Charge carrier separation in solar cells. IEEE J. Photovoltaics *5*, 461–469.

63. Lin, F., and Boettcher, S.W. (2014). Adaptive semiconductor/electrocatalyst junctions in water-splitting photoanodes. Nat. Mater. *13*, 81–86.

64. Hamann, T.W. (2014). An adaptive junction. Nat. Mater. *13*, 3–4.

65. Peter, L.M., Wijayantha, K.G.U., and Tahir, A.A. (2012). Kinetics of light-driven oxygen evolution at α-Fe_2O_3 electrodes. Faraday Discuss *155*, 309–322.

66. Wang, Z., Lyu, M., Chen, P., Wang, S., and Wang, L. (2018). Energy loss analysis in photoelectrochemical water splitting: a case study of hematite photoanodes. Phys. Chem. Chem. Phys. *20*, 22629–22635.

67. Cowan, A.J., Barnett, C.J., Pendlebury, S.R., Barroso, M., Sivula, K., Grätzel, M., Durrant, J.R., and Klug, D.R. (2011). Activation energies for the rate-limiting step in water photooxidation by nanostructured α-Fe_2O_3 and TiO_2. J. Am. Chem. Soc. *133*, 10134–10140.

68. Klahr, B., Gimenez, S., Fabregat-Santiago, F., Hamann, T., and Bisquert, J. (2012). Water oxidation at hematite photoelectrodes: the role of surface states. J. Am. Chem. Soc. *134*, 4294–4302.

69. Du, C., Zhang, M., Jang, J.-W., Liu, Y., Liu, G.-Y., and Wang, D. (2014). Observation and alteration of surface states of hematite photoelectrodes. J. Phys. Chem. C *118*, 17054–17059.

70. Ponomarev, E.A., and Peter, L.M. (1995). A comparison of intensity modulated photocurrent spectroscopy and photoelectrochemical impedance spectroscopy in a study of photoelectrochemical hydrogen evolution at p-InP. J. Electroanal. Chem. *397*, 45–52.

71. Le Formal, F., Pastor, E., Tilley, S.D., Mesa, C.A., Pendlebury, S.R., Grätzel, M., and Durrant, J.R. (2015). Rate law analysis of water oxidation on a hematite surface. J. Am. Chem. Soc. *137*, 6629–6637.

72. Pyun, C.W. (1971). Steady-state and equilibrium approximations in chemical kinetics. J. Chem. Educ. *48*, 194.

73. Gärtner, W.W. (1959). Depletion-layer photoeffects in semiconductors. Phys. Rev. *116*, 84–87.

74. Teodor, A.H., and Bruce, B.D. (2020). Putting photosystem I to work: truly green energy. Trends Biotechnol. *38*, 1329–1342.

75. Xuan, M., and Li, J. (2021). Photosystem II-based biomimetic assembly for enhanced photosynthesis. Natl. Sci. Rev. *8*, nwab051.

76. Carey, A.M., Zhang, H., Mieritz, D., Volosin, A., Gardiner, A.T., Cogdell, R.J., Yan, H., Seo, D.K., Lin, S., and Woodbury, N.W. (2016). Photocurrent generation by photosynthetic purple bacterial reaction centers interfaced with a porous antimony-doped tin oxide (ATO) electrode. ACS Appl. Mater. Interfaces *8*, 25104–25110.

77. McConnell, I., Li, G., and Brudvig, G.W. (2010). Energy conversion in natural and artificial photosynthesis. Chem. Biol. *17*, 434–447.

78. Noji, T., Matsuo, M., Takeda, N., Sumino, A., Kondo, M., Nango, M., Itoh, S., and Dewa, T. (2018). Lipid-controlled stabilization of charge-separated states ($P^+Q_B^-$) and photocurrent generation activity of a light-harvesting–reaction center core complex (LH1-RC) from *Rhodopseudomonas palustris*. J. Phys. Chem. B *122*, 1066–1080.

79. Feifel, S.C., Stieger, K.R., Lokstein, H., Lux, H., and Lisdat, F. (2015). High photocurrent generation by photosystem I on artificial interfaces composed of π-system-modified graphene. J. Mater. Chem. A *3*, 12188–12196.

80. Moore, G.F., and Brudvig, G.W. (2011). Energy conversion in photosynthesis: a paradigm for solar fuel production. Annu. Rev. Condens. Matter Phys. *2*, 303–327.

81. Chen, H.-Y., and Ardo, S. (2018). Direct observation of sequential oxidations of a titania-bound molecular proxy catalyst generated through illumination of molecular sensitizers. Nat. Chem. *10*, 17.

82. Seefeldt, L.C., Hoffman, B.M., Peters, J.W., Raugei, S., Beratan, D.N., Antony, E., and Dean, D.R. (2018). Energy transduction in nitrogenase. Acc. Chem. Res. *51*, 2179–2186.

83. Seefeldt, L.C., Peters, J.W., Beratan, D.N., Bothner, B., Minteer, S.D., Raugei, S., and Hoffman, B.M. (2018). Control of electron transfer in nitrogenase. Curr. Opin. Chem. Biol. *47*, 54–59.

84. Beiler, A.M., and Moore, G.F. (2018). Caught in the act. Nat. Chem. *10*, 3–4.

85. Kempler, P.A., Richter, M.H., Cheng, W.-H., Brunschwig, B.S., and Lewis, N.S. (2020). Si microwire-array photocathodes decorated with Cu allow CO_2 reduction with minimal parasitic absorption of sunlight. ACS Energy Lett. *5*, 2528–2534.

86. Trotochaud, L., Mills, T.J., and Boettcher, S.W. (2013). An optocatalytic model for semiconductor–catalyst water-splitting photoelectrodes based on in situ optical measurements on operational catalysts. J. Phys. Chem. Lett. *4*, 931–935.

87. Zhu, K., Ma, D., and Boettcher, S.W. (2020). Energy spotlight. ACS Energy Lett. *5*, 2739–2741.

88. Wadsworth, B.L., Nguyen, N.P., Nishiori, D., Beiler, A.M., and Moore, G.F. (2020). Addressing the origin of photocurrents and fuel production activities in catalyst-modified semiconductor electrodes. ACS Appl. Energy Mater. *3*, 7512–7519.

89. Li, H., Buesen, D., Dementin, S., Léger, C., Fourmond, V., and Plumeré, N. (2019). Complete protection of O_2-sensitive catalysts in thin films. J. Am. Chem. Soc. *141*, 16734–16742.

90. Bartlett, P.N., and Pratt, K.F.E. (1995). Theoretical treatment of diffusion and kinetics in amperometric immobilized enzyme electrodes. Part I: redox mediator entrapped within the film. J. Electroanal. Chem. *397*, 61–78.

91. Andrieux, C.P., Dumas-Bouchiat, J.-M., and Savéant, J.-M. (1980). Catalysis of electrochemical reactions at redox polymer electrodes. Effect of the film thickness. J. Electroanal. Chem. *114*, 159–163.

92. Andrieux, C.P., Dumas-Bouchiat, J.-M., and Savéant, J.-M. (1982). Catalysis of electrochemical reactions at redox polymer electrodes. J. Electroanal. Chem. Interfacial Electrochem. *131*, 1–35.

93. Chen, K., and Arnold, F.H. (2020). Engineering new catalytic activities in enzymes. Nat. Catal. *3*, 203–213.

94. Vaissier Welborn, V., and Head-Gordon, T. (2019). Computational design of synthetic enzymes. Chem. Rev. *119*, 6613–6630.

95. Noren, C.J., Anthony-Cahill, S.J., Griffith, M.C., and Schultz, P.G. (1989). A general method for site-specific incorporation of unnatural amino acids into proteins. Science *244*, 182–188.

96. Huang, P.-S., Boyken, S.E., and Baker, D. (2016). The coming of age of de novo protein design. Nature *537*, 320–327.

97. Savéant, J.-M. (2008). Molecular catalysis of electrochemical reactions. Mechanistic aspects. Chem. Rev. *108*, 2348–2378.